Spectro-mechanical Characterizations of Kerogen Heterogeneity and Mechanical Properties of Source Rocks at 6 nm Spatial Resolution

Devon S. Jakob, Le Wang, Haomin Wang, and Xiaoji G. Xu*

Department of Chemistry, Lehigh University, 6 E. Packer Ave., Bethlehem, PA, 18015, U.S.A.

*Corresponding Email:

Xiaoji G. Xu: xgx214@lehigh.edu

Abstract

In-situ measurements of the chemical compositions and mechanical properties of kerogen help understand the formation, transformation, and utilization of organic matter in oil shale source rocks. However, the optical diffraction limit prevents attainment of nanoscale resolution using conventional spectroscopy and microscopy. Here, we developed peak force infrared (PFIR) microscopy for multimodal characterization of kerogen in organic shales. PFIR microscopy provides correlative infrared imaging, mechanical mapping, and broadband infrared spectroscopy capabilities with 6 nm spatial resolution within the frequency region of 2400 to 4000 cm^{-1}. We have observed nanoscale heterogeneity in the chemical composition, aromaticity, and the level of maturity of the kerogens from source rocks obtained from the Eagle Ford shale play in Texas. The level of aromaticity of the kerogen positively correlates with the local mechanical moduli of the surrounding inorganic matrix, offering insights into the effect of kerogen heterogeneity on the nanoscale mechanical properties of the source rock. Our method and investigation advances the understanding towards the origin and transformation of kerogen in geological settings.

Introduction

The extraction and utilization of organic matters (kerogen) from underground shale formations into usable petroleum and natural gas has recently become a rapidly growing means of energy production throughout the world.[1,2] Organic matter is extracted by hydraulic fracturing (colloquially known as "fracking"), in which high-pressure liquids are pumped into the underground oil shale reservoirs to mechanically fracture it, creating fissures that allow gaseous and liquid hydrocarbons to escape and be collected at the surface. Kerogen is composed of both saturated and unsaturated hydrocarbon compounds that constitute anywhere from 1% to 15% or more of shale formations by weight. Fine-grained mineral particles such as quartz and clays form the inorganic matrix encapsulating the kerogen.[3] Given the economic importance of fracking and the rising energy demands worldwide, the geophysical and geochemical processes underlying the chemical transformation of organic precursors into usable hydrocarbons has been a major interest for understanding the evolution of quality oil shale plays.[4-6] Until recently, these models have been primarily limited to the effects that macroscopic properties, such as temperature, depth, pressure, and time, have on the quality of an oil shale reservoir.[7-10] These factors are generally well-understood and contribute to our estimations of recoverable oil shale reserves. Recent studies have begun to introduce more complex parameters into their models, such as total organic content, clay content, microcracks, anisotropy, level of thermal maturation, and overall porosity.[11-15] Special attention has been given to the effect of structural heterogeneity on the mechanical properties (modulus) of source rocks.[16,17] However, such models are incomplete as they are often based on results from scanning electron microscopy (SEM), Rock-Eval pyrolysis, and vitrinite reflectance measurements.[18] These conventional methods have intrinsic limitations which prevent them from recovering important information at spatial scales below the optical diffraction limit. Due to the lack of a suitable high-resolution analytical characterization technique with both chemical and mechanical sensitivity, direct correlations between structural anisotropy and mechanical properties below the optical diffraction limit have been limited to predictions based on investigations at larger spatial scales.[19-22] Direct nanoscale investigations into the chemical and mechanical heterogeneity of source rocks are the next challenge in obtaining more advanced geophysical and geochemical models of viable reservoir formations.

Kerogen within mature source rocks exists within nanopores throughout the source rock matrix.[23] One underexplored area of research is the effect of nanoscale kerogen heterogeneity on the formation of nanopores through the maturation process: what effect does the surrounding physical properties of the source rock have on kerogen heterogeneity and the gas potential of the reservoir? Currently, the influence of local factors such as the size, chemical identity, and mechanical properties of kerogen pores on the mechanical properties of the surrounding matrix is not well understood, as the nanopores are smaller than the spatial resolution of traditional spectroscopic methods. The optical diffraction limit binds traditional infrared microscopy and Raman microscopy to a half of the wavelength of light, which is approximately several microns or several hundred nanometers, respectively.[24] SEM, on the other hand, provides high spatial resolution over a large area, but it lacks chemical specificity for kerogens and requires vacuum conditions. High-energy electrons may alter or damage the sample.[25,26] Routine chemical analytical techniques such as gas or liquid chromatography, coupled with mass spectrometry, can reveal the identity of the kerogens.[27] These methods, however, are destructive. Generally, they require macroscopic amounts of samples and are unable to deliver the spatial anisotropy within the source rock.[28,29] Nuclear magnetic resonance studies can reveal the chemical structures of compounds within the source rock, but the spatial heterogeneity of the compounds throughout the sample is unobtainable with this method. Moreover, Nuclear magnetic resonance methods are often destructive due to the required injection and extraction of liquid which could potentially damage the structure of the porous source rock samples.[30,31] None of these methods can determine mechanical information (e.g. modulus) at any spatial scale, which prevents the correlative chemical and mechanical measurements needed to elucidate the mechanical effects of kerogen maturation and transformation.

Recently, two atomic force microscopy (AFM) based infrared microscopy methods have been applied to the study of organic shales. Photothermal induced resonance (PTIR, also commercially known as AFM-IR) spectroscopy has been coupled with traditional petrographic methods to characterize the microscale heterogeneity of organic matter.[32] However, the AFM-IR technique provides only ~ 100 nm spatial resolution on source rocks, insufficient to image the nanopores and kerogen within. Additionally, the AFM contact mode in which the PTIR operates in is vulnerable to tip wear when scanning over the rigid and rough surface of unpolished source rocks. The rough and unpolished surface of the source rock also prevents applications with tip-enhanced Raman

spectroscopy,[33] where the pristine condition of the metallic tip is required for optical enhancement. Scattering-type scanning near-field optical microscopy (s-SNOM), coupled with a synchrotron light source, reveals the chemical heterogeneity at an improved spatial resolution of 10 ~ 20 nm.[34] However, s-SNOM operates in the AFM tapping mode, which is unable to provide quantitative mechanical information. The synchrotron radiation source is also restricted for large research facilities and not suitable for possible field deployment. Besides, organic matters produce only very weak signals in s-SNOM measurements, compared with those using photothermal-based techniques. Moreover, another AFM based technique, Peak Force Quantitative Nanomechanical Mapping (Peak Force QNM) has been recently applied to the study of organic-rich shales to investigate the nanomechanical properties with a spatial resolution of a few nanometers. The mechanical measurements obtained through Peak Force QNM agreed well with predictions obtained through the model, indicating the possibility of predicting shale properties based on nanoscale measurements.[35] However, the Peak Force QNM is just mechanical characterization that lacks chemical specificity capabilities, meaning that the correlations of the chemical heterogeneity of kerogen and the physical properties of the source rock at the nanoscale have yet to be explored by Peak Force QNM.

To overcome the limitations of previous analytical techniques, we utilize peak force infrared (PFIR) microscopy to address the need for multimodal non-destructive characterizations of kerogen in source rocks with minimal sample preparation. PFIR microscopy is an AFM-based infrared imaging technique recently developed by our research group. It provides non-destructive and simultaneous infrared imaging and mechanical mapping, in addition to broadband spectroscopy, all at < 10 nm spatial resolution.[36] The non-destructive nature of PFIR allows the same sample to be measured numerous times without affecting the properties of the sample or destroying it. This advantage is beneficial over Rock-Eval pyrolysis, which requires the sample to be heated to hundreds of degrees Celsius to characterize the chemical composition. The scheme of the home-built PFIR microscopy apparatus with frequency coverage between 2000 cm^{-1} to 4000 cm^{-1} is depicted in **Fig. 1** and described in the *Experimental Section*. The local photothermal expansion from infrared absorption, which is characteristic of the chemical heterogeneity of kerogen, is transduced by the mechanical response of the AFM cantilever. The peak force tapping mode of AFM, in which PFIR microscopy is operated, measures the moduli of the sample surface. The correlative infrared and mechanical responses enable us to decipher possible correlations between

kerogen moieties and local matrix properties. The characteristic infrared absorption of saturated and unsaturated hydrocarbon reveals the nanoscale aromaticity and enables further deduction of the in-situ maturity of the kerogen in the source rocks.

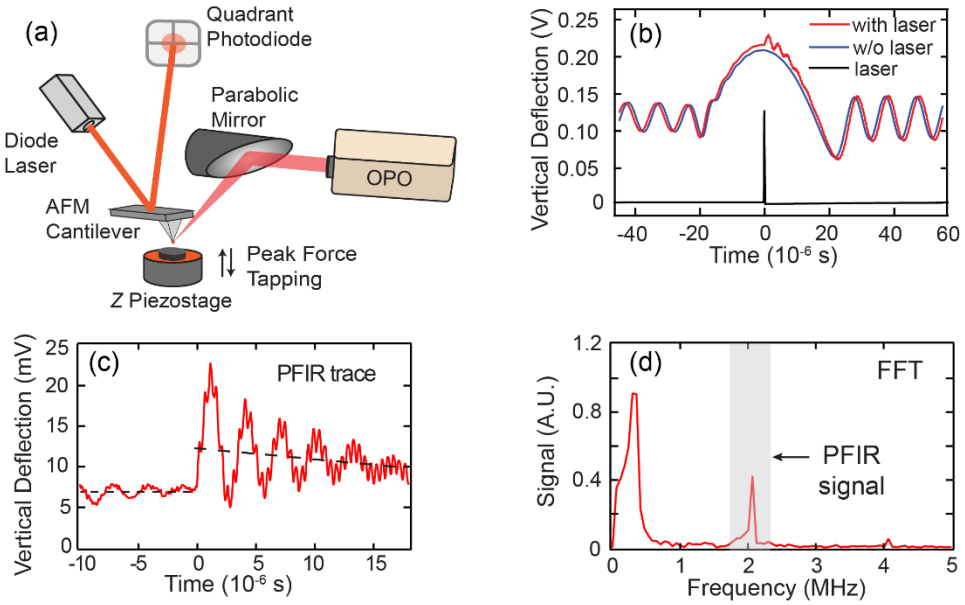

Figure 1. Experimental scheme of PFIR microscope and data collection. (a) Experimental setup of the PFIR apparatus used for infrared and mechanical characterization of kerogen in source rocks. (b) The cantilever deflection curve measured with laser-induced contact resonance (red curve) and subsequently without the laser-induced contact resonance. (blue curve) (c) The laser-induced mechanical response of the cantilever from the photothermal expansion of the sample after background subtraction to produce the PFIR trace. The contact resonance of the cantilever is excited due to rapid thermal expansion of the sample from absorption of the pulsed infrared laser. (d) Subsequent fast-Fourier transform on the PFIR trace to obtain the contact resonance band, which is integrated and used as the PFIR signal.

Experimental Section

The scheme of the home-build peak force infrared microscopy apparatus is depicted in **Fig. 1**. The details of the optical setup are described in a recent paper published by our group.[36] An atomic force microscope (Multimode AFM with Nanoscope V, Bruker) is operated in the peak force tapping (PFT) mode.[37] In PFT mode, the AFM cantilever is held stationary and the sample surface

is oscillating vertically at a low frequency (typically 4 kHz) by a piezo state. (**Fig. 1a**) Near the upper turning point of the sample oscillation, the AFM tip momentarily contacts the surface of the sample, and the AFM cantilever is pushed upward, leading to vertical deflections. The maximal vertical deflection of the cantilever is used as the set point in the PFT feedback mechanism. After momentary contact, the sample surface is lowered by the piezo stage to finish one PFT cycle. PFT feedback maintains a controlled tip-indentation on the sample surface for each PFT cycle to avoid tip-wear. Infrared pulses of 10 ns duration from a frequency tunable optical parametric oscillator (OPO, NT277, EKSPLA) are synchronized with the PFT cycles at half of the PFT frequency. The OPO laser provides continuously tunable wide infrared radiation coverage (between 2400 to 4000 cm^{-1}) to saturated and unsaturated hydrocarbon (C-H) bonds, which is not accessible for current popular quantum cascade lasers. The spectral resolution of the OPO is 10 cm^{-1} that determines the spectral resolution of the method. Photothermal expansions of the sample are generated by the laser at every other peak force tapping cycle and transduced by the cantilever deflection of the AFM. (**Fig. 1b**) Cantilever responses from the PFT cycle without laser excitation is recorded as a reference for background subtraction. (**Fig. 1c**) The contact resonance oscillation is observed at ~ 2 MHz and its amplitudes is extracted through Fourier transform to obtain the PFIR signal during each PFT cycle. (**Fig. 1d**) The larger peak at ~275 kHz corresponds to the free oscillation frequency of the AFM cantilever (HQ:NSC15, Mikromasch). The PFIR image is formed by collections of the PFIR signal at a fixed laser frequency as the AFM tip is scanned over the source rock sample. The PFIR spectrum is collected by the sweeping the frequency of the OPO when the AFM tip is stationary at a location of interest. The complementary images of modulus and adhesion are derived from the Derjaguin-Muller-Toporov contact mechanical model from the cantilever deflection after tip-sample contact.[38] In this model, the reduced Young's modulus (E^*) is related to the peak force (F_{pf}), the adhesion force (F_{ad}), the sample deformation ($d - d_0$), and the tip radius (R) by

$$F_{pf} - F_{ad} = \frac{4}{3} E^* \sqrt{R(d - d_0)^3} \quad (1)$$

The tip radius of the probe used in the measurements is found by identifying spatial frequencies from a scan on a rough polycrystalline titanium calibration sample, following the standard tip-quantification procedure of the Bruker AFM. The reduced Young's modulus can be used to find

Young's modulus of the sample, assuming that the tip modulus (E_{tip}) is infinite, given that the Poisson's ratio for the sample (υ_s) is known by

$$E^* = \left[\frac{1-\upsilon_s^2}{E_s} + \frac{1-\upsilon_{tip}^2}{E_{tip}}\right]^{-1} \quad (2)$$

However, the Poisson's ratio is generally not precisely known, it is typical to report the reduced modulus.[39] Quantitative measurements of modulus are achieved through the absolute method of measuring the tip radius, spring constant, and deflection sensitivity prior to the experiment.

Immature source rock samples used in this study were obtained from the Eagle Ford shale play in southwest Texas. The core samples were pulverized into fine powders (10 to 25 μm, determined by an optical microscope) and mechanically pressed under 6000 psi to reconstitute the samples into flat pellets of two parallel surface for the PFIR measurements. Samples with two parallel surfaces are required for the AFM instrument. This method is similar to the KBr pellet method of sample preparation that has been widely used in previous spectroscopic petrography studies.[32,40-42] Here, we reconstituted the powders into pellets without using KBr, so that the true topographic and mechanical information could be extracted. PFIR images were measured on sample surfaces measuring 3 μm × 3 μm over multiple grains. PFIR images were completed in the PFT mode at a scan rate of 0.2 Hz, a peak force set point of 9 nN, a PFT frequency of 4 kHz, and a sample oscillation amplitude between 50 to 90 nm, depending on sample roughness. PFIR images were obtained in approximately 40 minutes each. Signal was collected in real time with a data acquisition card (PXI-5122, National Instruments) at a 50 M samples/second sampling rate. The complementary topography, adhesion, and modulus maps were collected at a PFT frequency of 2 kHz. These measurements were obtained separately from the PFIR measurements to eliminate any possible signal cross-talk between photothermal expansion and AFM probe indentation.

Results

PFIR microscopy reveals the distribution of infrared responses from kerogen in immature oil shale source rocks together with correlative mechanical properties of reduced Young's modulus and adhesion. The PFIR measurements are displayed in **Fig. 2**. The topography of the sample (shown

in **Fig. 2a**) reveals the surface roughness of a 3 μm × 3 μm region. Note that because the sizes of pulverized grain are between 10 μm and 25 μm, the measurement area is likely to be on a single grain. Adhesion (**Fig. 2b**) and modulus (**Fig. 2c)** images provide the mechanical properties of the same region. The topography and mechanical images do not provide indications to chemical compositions. The distribution of saturated hydrocarbons (shown in **Fig. 2d**) is revealed by the PFIR microscopy at the infrared frequency of 2920 cm^{-1} that is characteristic of alkyl CH_2 asymmetric stretching. Similarly, the distribution of the unsaturated hydrocarbons (displayed in **Fig. 2e-f**) is revealed at the infrared frequency of 3032 cm^{-1}, which is resonant with the unsaturated CH stretching. Spectroscopic contrasts within each image indicate that kerogens of varying chemical identity are spatially localized within the sample at the nanoscale. The infrared frequencies of 2920 cm^{-1} and 3032 cm^{-1} are chosen as they can be differentiated within the accompanying spectra and do not overlap with other infrared-active species found within source rocks. These two frequency responses allow us to affirm the identities of kerogen as containing either unsaturated hydrocarbons, saturated hydrocarbons, or both if the signal overlap is present in images or spectra.

Individual point spectra (**Fig. 2g**) are taken to further elucidate the identity of the kerogen. The collection of PFIR spectra was achieved by sweeping the frequency of the OPO while the AFM probe remained at a location of interest while under PFT mode feedback. The PFIR signal from the contact resonance normalized by the laser power was plotted versus the infrared frequency to form the PFIR spectrum. Distinct chemical identities are revealed throughout the sample surface, as suggested by the differences from point spectra. The spectrum originating from the 2920 cm^{-1} active area (gray spectrum) further supports the notion that PFIR signal in **Fig. 2d** originates from saturated hydrocarbon-rich kerogen due to the pronounced peak at 2920 cm^{-1}. The incomplete

separation of the peaks at 2920 cm^{-1} and 2870 cm^{-1}, which are typical resonances of aliphatic hydrocarbons, is attributed to two sources. Kerogen is a mixture of numerous aliphatic hydrocarbon moieties which leads to the inhomogeneous broadening of the two peaks typically seen for aliphatic hydrocarbons. This effect is coupled with the relatively low spectral resolution of our light source (10 cm^{-1}), further convoluting the two standard aliphatic peaks. The red arrow is shown in **Fig. 2d** indicating a location that is low in saturated concentration, despite the point spectrum showing a large concentration of saturated functional groups (2920 cm^{-1}). It is important to note that the spectra shown in **Fig. 2g** are normalized to each other and offset. The important characteristics shown by the spectra are the relative differences between the saturated absorption (2920 cm^{-1}) and the unsaturated absorption (3032 cm^{-1}) within each spectrum.

The spectra taken at the 3032 cm^{-1} areas in **Fig. 2e** (red, blue, and green spectra) show the presence of unsaturated rich constituents within the source rocks. In these studies, the PFIR signal at 3032 cm^{-1} is much weaker than the signal at 2920 cm^{-1}. This observation can be attributed to relatively low aromaticity or concentration of unsaturated hydrocarbons. The common absorption at ~3250 cm^{-1} likely corresponds to the N-H stretching mode for nitrogen-containing compounds within the immature kerogen.

A spatial resolution of 6 nm is extracted from the cross-section marked in **Fig. 2f** as the width between the edge height of the PFIR signal. Similarly, the spatial resolution of the modulus and adhesion images are extracted and shown in **Fig. S3**. The apex radius of the probe used in this measurement is found to be 30 nm, following the standard tip-quantification procedure of the Bruker AFM.[36] The spatial resolution of PFIR surpasses the tip radius because the tip-sample contact area in the peak force tapping mode is smaller than the full probe radius due to small

indentations in each tip-sample contact cycle. Due to the similar spatial resolution between the PFIR and mechanical images, meaningful correlations between these images can be explored.

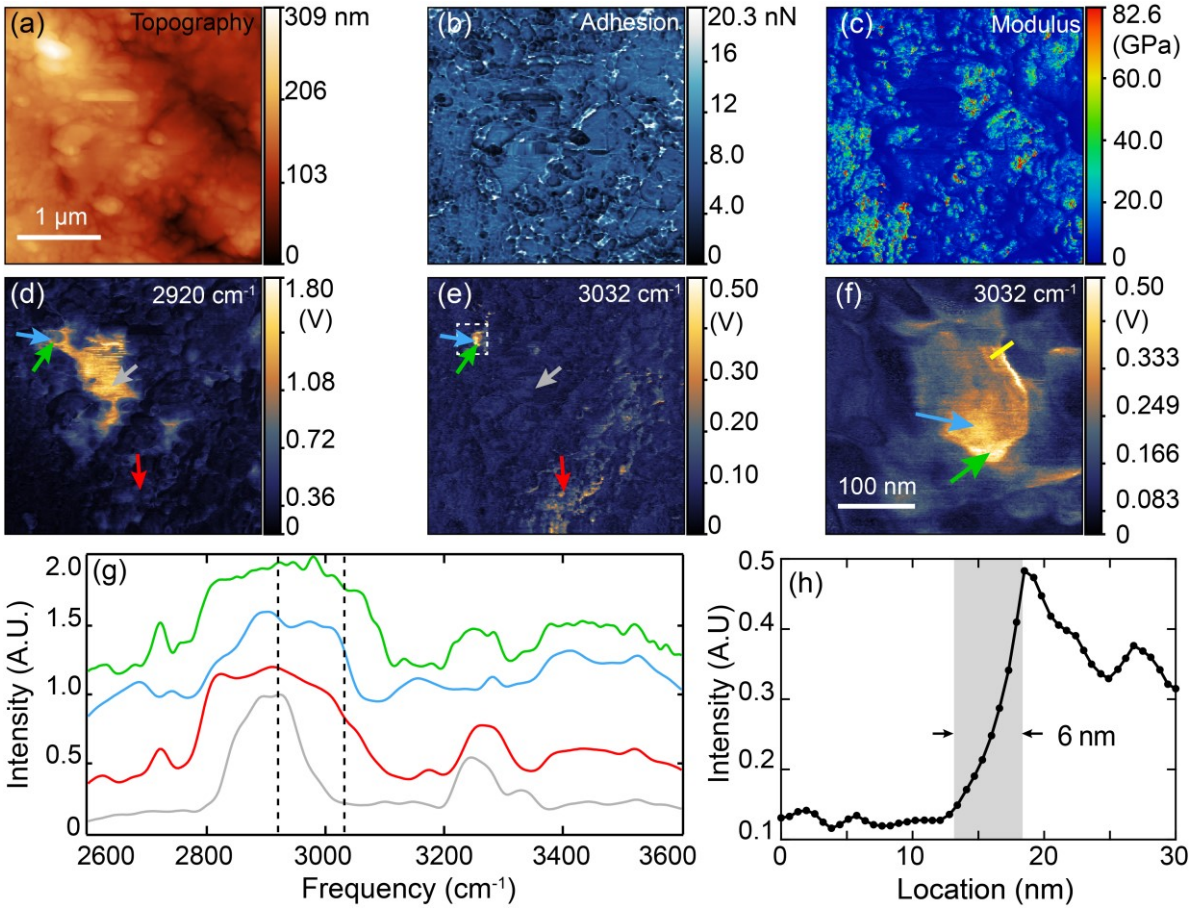

Figure 2. PFIR acquired images and point spectra of an immature 3 μm × 3 μm Eagle Ford source rock sample. (a) Topography of the source rock. The scale bar is 1 μm. (b) Adhesion between AFM tip and the sample. (c) Modulus map of the source rock sample surface. (d) PFIR image taken at 2920 cm^{-1}, indicating the presence of saturated hydrocarbon compounds. (e) PFIR image taken at 3032 cm^{-1}, characteristic of unsaturated compounds. (f) A 330 nm × 330 nm PFIR image taken at 3032 cm^{-1} positioned within the location of the white box in 2e. (g) Point spectra taken from chosen areas on the surface as indicated by the colored arrows in the accompanying PFIR images. (h) A spatial resolution of 6 nm is observed from a cross-section in (f), indicated by the yellow line.

The multimodal capability of PFIR microscopy allows establishing correlations between chemical signal and its accompanying mechanical signal. **Fig. 3** displays another multimodal PFIR measurement of the same oil shale source rock sample at a different 3 μm × 3 μm area located on a separate grain of powder, in which more unsaturated moieties are revealed than in the region of **Fig. 2**. **Fig. 3a** shows the topography of the region. The PFIR images from the saturated (**Fig. 3c**), unsaturated hydrocarbons (**Fig. 3d**), and accompanying modulus map (**Fig. 3b**) are processed to obtain the correlations between chemical compositions of kerogen pores and moduli of surrounding inorganic matrix. The spectral intensities at individual locations are correlated with the average moduli of their surroundings. **Fig. 3e** shows the average moduli of the surrounding of both saturated hydrocarbon and unsaturated hydrocarbon versus the distance from the hydrocarbons. The detailed procedure of the data processing is included in **Fig. S1.** The correlation between the surrounding moduli and the distance reveals that kerogen of saturated hydrocarbon correlates with low-modulus surroundings; in contrast, kerogen of unsaturated hydrocarbons correlates with high-modulus surroundings.

How should we understand such correlations? Assuming that the organic matter precursors of the kerogen from the 3 μm × 3 μm region have the same initial maceral composition (organic matters from ancient organisms), because of the small size of the region. Under external pressure, the high-modulus inorganic surroundings transfer higher pressure to the organic matters trapped within the inorganic matrix than low-modulus surroundings, leading to variations of local pressure levels on the initial maceral compositions. Variations of the local pressures at the nanometer to microscale lead different stages of organic matter in the maturation pathway. As the percentage of hydrogen reduces during maturation,[43] the density of organic matter increases. Unsaturated kerogen moieties have a higher density than saturated kerogens.[44,45] Different local pressures from the inorganic

matrix affect equilibria of chemical reactions that transform kerogens of saturated hydrocarbons into kerogens of unsaturated moieties over millions of years.[46] Described by Le Chatelier's principle, higher external pressure favors chemical species with smaller volume (or higher density) in chemical reactions. Therefore, the high-modulus inorganic matrix favors the generation of high-density kerogens of more unsaturated moieties than saturated moieties, which is supported by the observed correlations between the chemical identity and moduli of the surrounding inorganic matrix. Note that we do not rule out other factors in the chemical transformation of the kerogen, most notably the organic precursor composition. However, since the area of study (3 μm × 3 μm) is very small, macroscopic parameters such as the original depth of the sample, as well as the temperature and pressure experienced during the past millions of years are practically the same.

No correlation between the adhesion image and the PFIR images in **Fig. 2** was found. We believe the kerogen is buried slightly below the surface of the oil shale but within the field enhancement of the infrared light. Since adhesion is measured at the surface, there is no guarantee of clear correlation or anti-correlations between adhesion and chemical distributions. On the other hand, the level of correlations between maps of organic composition and adhesion may indicate whether the kerogen is enclosed within the rock or present at the surface. This aspect may provide insight toward the vertical nanoscale distribution of the kerogens in the source rock.

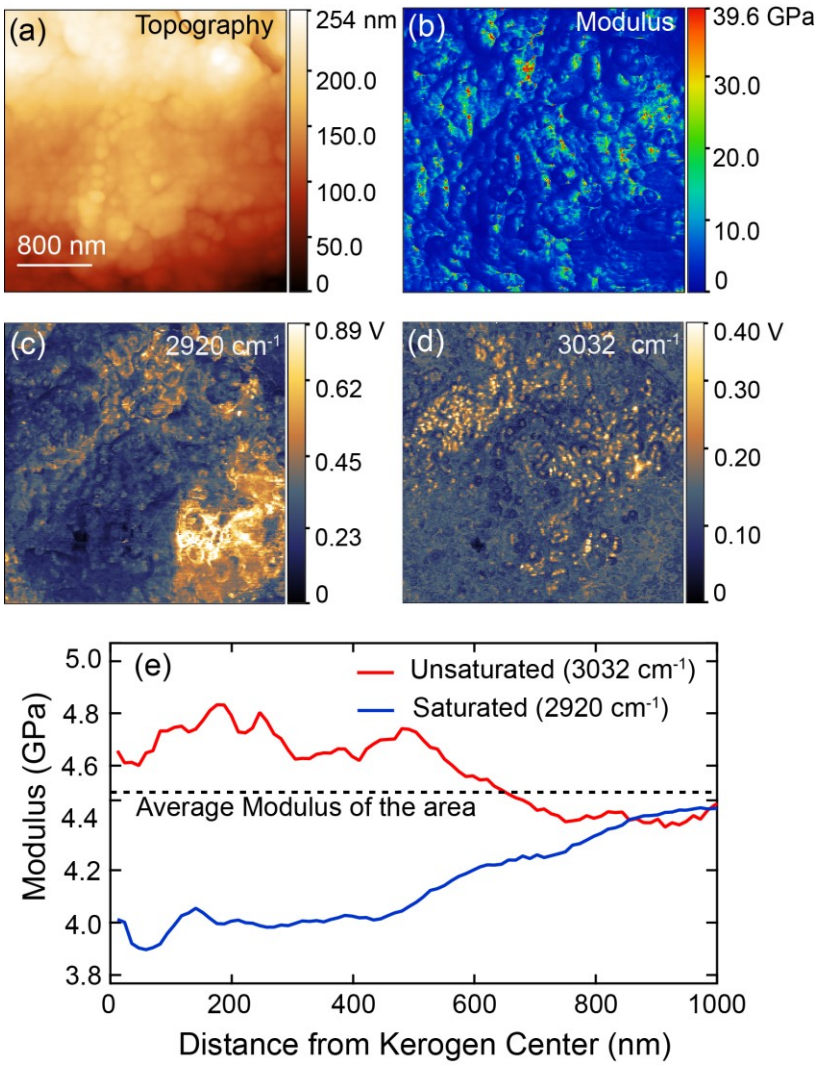

Figure 3. A correlation between chemical and mechanical observed with PFIR. (a) Topography obtained from a 3 μm × 3 μm area of an Eagle Ford shale source rock sample. The scale bar is 800 nm. (b) Modulus obtained over the same area. (c) PFIR image at 2920 cm^{-1} showing the presence of saturated hydrocarbon groups. (d) PFIR image at 3032 cm^{-1} showing the presence of unsaturated hydrocarbon groups. (e) Correlation between chemical identities and surrounding modulus values. Data from the unsaturated-modulus correlation are depicted in red and data from the saturated-modulus correlation are depicted in blue. The average modulus (4.5 GPa) is obtained by averaging the modulus over the entire image in (b).

We can also derive the aromaticity of the region of measurement. Aromaticity, the relative amount of carbon atoms in a sample that exist in unsaturated moieties, is an important factor for the utilization of the kerogen as it is a factor to the overall quality of oil shale. Aromaticity is also important when assessing the potential risks that fracking poses to surrounding water basins and watersheds, due to the carcinogenic nature of many organic unsaturated compounds.[47-49] The extracted numerical data from the chemical maps in **Fig. 3c-d** were normalized and plotted as a point-density map. Aromaticity was found with a method similar to that used by Craddock et al.[50] In our case, a heatmap is generated by extracting the signal magnitude of each pixel from the chemical maps in **Fig. 3c-d**. Since both maps correspond to the same sample area, the saturated absorption intensity at 2920 cm^{-1} can be plotted against the unsaturated absorption intensity at 3032 cm^{-1}. After normalization, the aromaticity can be calculated as $f_a = \frac{I_{3032}}{I_{3032}+I_{2920}}$. Data points less than 20% of maximum signal magnitude after normalization were attributed to the inorganic matrix and not used in determining aromaticity. **Fig. 4** displays the heatmap produced from correlating normalized intensities of saturated (2920 cm^{-1}) and unsaturated hydrocarbons (3032 cm^{-1}) from PFIR images as described above. This method establishes aromaticity of 0.13, typical to values reported previously of shales of the same origin.[32,51]

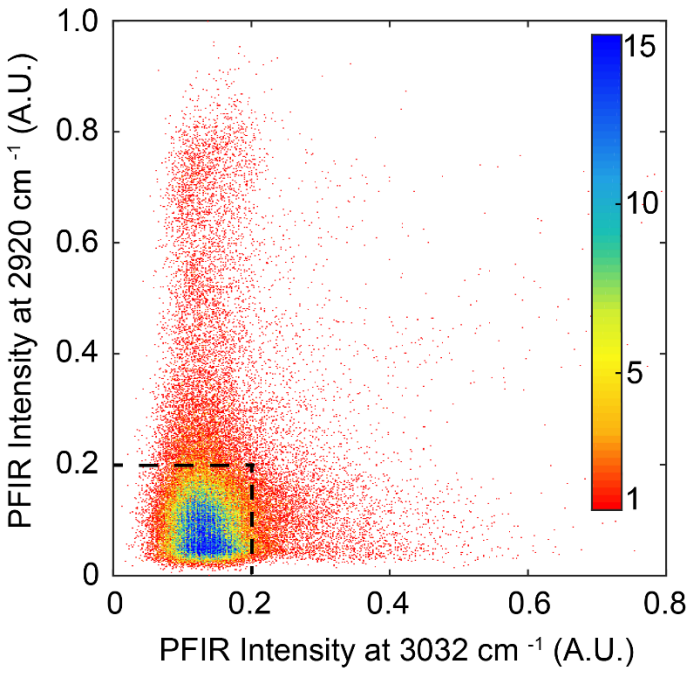

Figure 4. Aromaticity measurement obtained through PFIR. A heatmap of normalized PFIR signal intensities produced by plotting each individual pixel corresponding to PFIR intensity at 2920 cm^{-1} with the PFIR intensity at 3032 cm^{-1}. PFIR intensities accounting for the weakest 20% of the maximum signal are attributed to the inorganic matrix within the sample and is ignored for aromaticity calculation. The data is extracted from the measurement shown in **Fig. 3**.

The ratio between the saturated hydrocarbon and unsaturated hydrocarbon infrared responses allows us to derive the in-situ maturity of the kerogen at the nanoscale. The maturity of kerogen is an indicator of a reserves shale-oil production quality.[52,53] In FTIR characterization of oil shale, peak-ratios from infrared spectra correlate with the thermal maturity and classification of the kerogen within oil shale samples.[51,53,54] As previous literature and our measurements above have revealed, the maturity of kerogen varies greatly across sub-micron length scales.[32] Previous literature suggests that the elastic properties within sub-micron length scales result from variability in the rate of maturation within these areas.[55] However, measurement of the maturity of kerogen at spatial scales below the optical diffraction limit is inaccessible by traditional infrared

spectroscopy.[50,53,56] In contrast, the high spatial resolution of the PFIR microscopy and its ability to collect spectra at individual location enables the comparison of nanoscale macerals within the same sample. In our study, we collect PFIR spectra from eight locations on the sample of **Fig. 3** and four locations from **Fig. 2**. The locations of the measurements are marked in **Fig. S2**. PFIR spectra allow for the C-factor (the oxygenated character) and A-factor (the saturated character) to be obtained from normalized spectra by the creation of a van-Krevelen diagram. Van-Krevelen diagrams are commonly used in spectroscopic studies of oil shales and coals to depict the extent of chemical transformation of the kerogen towards natural gas, oil, and other energy-rich materials. The diagram uses infrared proxies to calculate the maturity of the oil shale samples. Here, the maturity of the kerogens was completed in a method according to that used by Ganz et al.[51] To obtain the relative saturated hydrocarbon content, the A-factor was calculated as $[I_{2920}]/[I_{2920} + I_{3032}]$ To obtain the relative oxygen content in each sampled area, the C-factor was calculated as $[I_{3645}]/[I_{2920} + I_{3032}]$. The sharp peak at around 3645 cm^{-1} was chosen for this calculation as it is indicative of the O-H stretching vibration. 2920 cm^{-1} and 3032 cm^{-1} result from saturated (CH_2 asymmetric stretching) and unsaturated (CH stretching) hydrocarbons groups, respectively. This method slightly differs from Ganz's method since 3645 cm^{-1} was chosen as the oxygenated band instead of 1710 cm^{-1} to ensure the laser spot size and focus of our OPO remains unchanged throughout the measurement. 3645 cm^{-1} is a common infrared absorption in many of the matrix components, which could potentially lead to overestimating the oxygen content. However, kerogen in oil shale exists in pores ranging from many nanometers to micrometers in diameter and is spatially separated from the mineral matrix. The high spatial resolution of PFIR ensures that the oxygen content from the mineral matrix can be avoided, by obtaining infrared spectra at the center of the kerogen pores. It is possible that the kerogen is buried underneath the shale surface but still

within the field enhancement of the infrared light by the metallic tip. In this case, the oxygen contribution from the mineral matrix components would be small, since the field enhancement is also small. **Fig. 5** shows the resulting van-Krevelen diagram of kerogen maturity obtained through analyzing peak ratios obtained at different locations along with the sampled areas. These specific areas were chosen since the PFIR images in **Figs. 2-3** indicated the presence of organic moieties of varying composition at these locations. In our study, the A-factors and C-factors are calculated through a method similar to other commonly employed methods.[32,50,51] The method of treatment is described in the *Experimental* S*ection*. The measurements reveal varying kerogen maturity from adjacent organic pockets. The organic matter within the Eagle Ford shale play is classified as type II kerogen, since the maceral composition originated primarily from plankton.[57] In typical van-Krevelen diagrams, the maturity of many oil shale samples are compared to each other after artificial maturation. This allows for a maturation pathway to be established for that sample.[51,58,59] However, our measurement provides the ability to estimate and compare the level of the maturity and reveals heterothe geneity of the maturity for individual macerals from the nanoscale. The importance of the observation here is that the maturity of individual macerals varies at the nanoscale, despite being subjected to the same pressure and temperature over geological time periods.

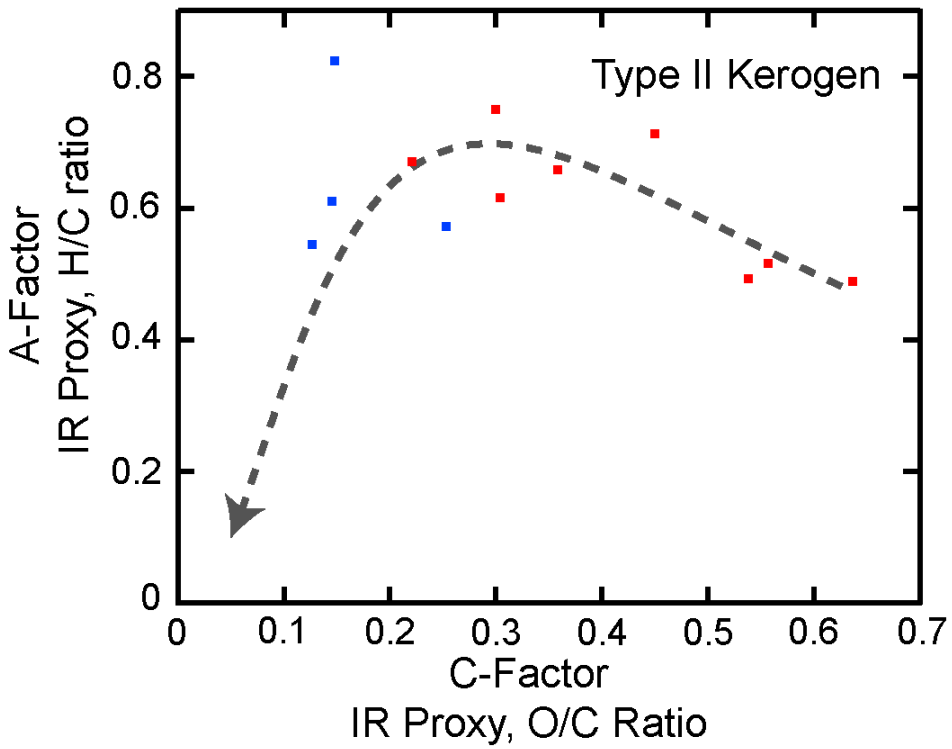

Figure 5. Van-Krevelen diagram obtained from PFIR point spectra. Twelve spectra of organic pockets within the Eagle Ford source rock sample are used to generate this plot in order to demonstrate the existence of nanoscale heterogeneity of the maturity states of the organic matters. The colors indicate two separate 3 μm × 3μm measurement regions, indicated in **Fig. S2**. The blue data points are obtained from locations within the area measured in **Fig. 2,** and the red data points show the measurements obtained from the location measured in **Fig. 3.** For each data point, the relative intensities of saturated functional groups (A-factor) are plotted against the relative intensities of oxygenated functional groups (C-factor) within a single point spectrum. The dashed line indicates the typical maturity pathway for Type-II kerogen as a guide, following a typical maturation pathway.

Discussion

PFIR microscopy is advantageous for investigations of oil shale source rocks, compared with the existing AFM-based infrared techniques. In our studies, to access the characteristic C-H

vibrational mode around 3000 cm^{-1}, we combine a frequency tunable optical parametric oscillator with our PFIR apparatus, which results in an infrared microscope that is capable of measuring an infrared bandwidth between 2400 cm^{-1} and 4000 cm^{-1} at 6 nm spatial resolution. In comparison, the QCL based nano-IR microscopies do not offer such a wide coverage at high-frequency mid-infrared range. The traditional PTIR technique also does not offer sub 10 nm spatial resolution. The 6 nm spatial resolution obtained from PFIR on source rocks is far greater than the ~100 nm spatial resolution of the AFM-IR technique[32,60] and the ~ 20 nm spatial resolution of s-SNOM.[34] The peak force tapping operational mode of PFIR is suitable for unpolished source rock surfaces, which are typically rough. In comparison, the contact mode AFM that the AFM-IR technique operates in cannot handle rough and sticky surfaces due to tip wear and sample scratches. The quantitative mechanical information from the peak force tapping in PFIR microscopy enables nanoscale correlations between the mechanical and chemical responses in one operational mode. In contrast, the tapping mode s-SNOM does not provide any access to the quantitative mechanical information of the sample. The chemical sensitivity of PFIR microscopy is advantageous over scanning electron microscopy or atomic force microscopy that only provides the morphology of the sample. In addition, PFIR microscopy is nondestructive to the sample and operates under ambient conditions, which is advantageous over the scanning electron microscopy that requires high-energy electrons and high-vacuum conditions or the commonly employed nuclear magnetic resonance which requires injection of liquid into the sample. PFIR microscopy is suitable for providing both chemical and mechanical information for organic source rock samples.

Our investigation on oil shale source rocks demonstrates the presence of nanoscale heterogeneity of the chemical compositions of kerogen and associated aromaticity and maturity. The correlation between the mechanical and chemical compositions revealed by our method suggests that the local

mechanical modulus of the inorganic matrix may influence the nanoscale chemical transformation of the kerogens. Higher modulus inorganic matrices favor the generation of kerogen with high unsaturated-moiety concentration over lower modulus inorganic matrix.

Further improvement of the PFIR microscopy measurement of kerogen can be made in several aspects. For example, statistical treatment can be used with multiple measurement of the same areas and locations to derive a confidence limit on the measured aromaticity and maturity. On the sample preparation procedure, instead of pulverizing the sample to create a pellet of parallel surfaces to satisfy the requirement of the AFM, the sample of source rock can be polished to create a parallel flat surface for the AFM. On the instrument side, infrared laser sources with narrower spectral bandwidth than the existing OPO can be used to improve the spectral resolution, so that the resonant peaks of the kerogen will be better resolved, and further spectral analysis procedures such as principal component analysis can be performed. Nonetheless, the purpose of work here is to first demonstrate the possibility and the opportunity of using PFIR microscopy for *in situ* studies of oil shale source rock. Fine-tuning of the method and instrument will be carried in continuing studies.

Conclusion

In summary, we have demonstrated that the PFIR microscopy is a non-destructive nanoscale-resolution multimodal infrared and mechanical characterization technique in the study of kerogen in oil shale source rocks. Using this method, nanoscale heterogeneity of chemical compositions, aromaticity, and maturity have been revealed and the aromaticity of the kerogen has been found to correlate with the local mechanical properties of the inorganic matrix. We hope that the high spatial resolution imaging/analytical methodology will constitute an important step to provide

additional chemical insight for detailed geochemical models aimed at understanding the origin and transformation of kerogen in geological settings.[55]

Acknowledgments

We would like to thank Mr. Paul Jakob for helpful discussions and for obtaining the shale samples. We would like to thank Dr. Kai Landskron for the pellet press for sample preparation. We would also like to thank Dr. Martin Wagner and Dr. Gray Bebout for proofreading this article and insightful conversations. This work was supported by the Beckman Young Investigator Program and the National Science Foundation (CHE-1847765).

Author contributions

X.G.X and D.S.J. conceived the original idea. L.W., H. W. and X.G.X. built the prototype of the instrument. D.S.J. collected the experimental data. D.S.J., X.G.X participated in the data analysis. X.G.X. and D.S.J. wrote the manuscript. L.W. and H.W. helped edit the manuscript.

Competing Interests

The authors declare no competing financial or non-financial interests.

Supporting Information

Method to extract average modulus values using pixel indices from PFIR images, locations of collected point spectra obtained for the van-Krevelen diagram shown in **Fig. 5**, and the spatial resolution measurement of modulus mapping from **Fig. 2**.

References:

(1) Cueto-Felgueroso, L.; Juanes, R. "Forecasting long-term gas production from shale". *Proc. Natl. Acad. Sci.* **2013**, *110*, 19660-19661.
(2) Kerr, R. A. "Natural Gas From Shale Bursts Onto the Scene". *Science* **2010**, *328*, 1624-1626.
(3) Soeder, D. J. "The Marcellus shale: Resources and reservations". *Eos, Transactions American Geophysical Union* **2010**, *91*, 277-278.
(4) Vandenbroucke, M.; Largeau, C. "Kerogen origin, evolution and structure". *Org. Geochem.* **2007**, *38*, 719-833.

(5) Behar, F.; Vandenbroucke, M. "Chemical modelling of kerogens". *Org. Geochem.* **1987**, *11*, 15-24.
(6) Craddock, P. R.; Bake, K. D.; Pomerantz, A. E. "Chemical, Molecular, and Microstructural Evolution of Kerogen during Thermal Maturation: Case Study from the Woodford Shale of Oklahoma". *Energy Fuels* **2018**, *32*, 4859-4872.
(7) Pepper, A. S.; Corvi, P. J. "Simple kinetic models of petroleum formation. Part I: oil and gas generation from kerogen". *Mar. Pet. Geol.* **1995**, *12*, 291-319.
(8) Tissot, B.; Durand, B.; Espitalie, J.; Combaz, A. "Influence of nature and diagenesis of organic matter in formation of petroleum". *AAPG Bull.* **1974**, *58*, 499-506.
(9) Tissot, B.; Pelet, R.; Ungerer, P. "Thermal history of sedimentary basins, maturation indices, and kinetics of oil and gas generation". *AAPG Bull.* **1987**, *71*, 1445-1466.
(10) El Nady, M. M.; Ramadan, F. S.; Hammad, M. M.; Lotfy, N. M. "Evaluation of organic matters, hydrocarbon potential and thermal maturity of source rocks based on geochemical and statistical methods: Case study of source rocks in Ras Gharib oilfield, central Gulf of Suez, Egypt". *Egypt. J. Pet.* **2015**, *24*, 203-211.
(11) Shitrit, O.; Hatzor, Y. H.; Feinstein, S.; Vinegar, H. J. "Acoustic and petrophysical evolution of organic-rich chalk following maturation induced by unconfined pyrolysis". *Rock Mech. Rock Eng.* **2017**, *50*, 3273-3291.
(12) Zhao, L.; Qin, X.; Han, D.-H.; Geng, J.; Yang, Z.; Cao, H. "Rock-physics modeling for the elastic properties of organic shale at different maturity stages". *Geophysics* **2016**, *81*, D527-D541.
(13) Avseth, P.; Mukerji, T.; Mavko, G.; Dvorkin, J. "Rock-physics diagnostics of depositional texture, diagenetic alterations, and reservoir heterogeneity in high-porosity siliciclastic sediments and rocks—A review of selected models and suggested work flows". *Geophysics* **2010**, *75*, 75A31-75A47.
(14) Suarez-Rivera, R.; Fjær, E. "Evaluating the poroelastic effect on anisotropic, organic-rich, mudstone systems". *Rock Mech. Rock Eng.* **2013**, *46*, 569-580.
(15) Zhu, Y.; Xu, S.; Payne, M.; Martinez, A.; Liu, E.; Harris, C.; Bandyopadhyay, K. In *SEG Technical Program Expanded Abstracts 2012*; Society of Exploration Geophysicists, 2012, pp 1-5.
(16) Sayers, C. M. "The effect of anisotropy on the Young's moduli and Poisson's ratios of shales". *Geophys. Prospect.* **2013**, *61*, 416-426.
(17) Sone, H.; Zoback, M. D. "Mechanical properties of shale-gas reservoir rocks—Part 1: Static and dynamic elastic properties and anisotropy". *Geophysics* **2013**, *78*, D381-D392.
(18) Shitrit, O.; Hatzor, Y. H.; Feinstein, S.; Palchik, V.; Vinegar, H. J. "Effect of kerogen on rock physics of immature organic-rich chalks". *Mar. Pet. Geol.* **2016**, *73*, 392-404.
(19) Ortega, J. A.; Ulm, F.-J.; Abousleiman, Y. "The effect of the nanogranular nature of shale on their poroelastic behavior". *Acta Geotech.* **2007**, *2*, 155-182.
(20) Sayers, C. "The elastic anisotrophy of shales". *J. Geophys. Res.: Solid Earth* **1994**, *99*, 767-774.
(21) Vasin, R. N.; Wenk, H. R.; Kanitpanyacharoen, W.; Matthies, S.; Wirth, R. "Elastic anisotropy modeling of Kimmeridge shale". *J. Geophys. Res.: Solid Earth* **2013**, *118*, 3931-3956.
(22) Jakobsen, M.; Hudson, J. A.; Johansen, T. A. "T-matrix approach to shale acoustics". *Geophys. J. Int.* **2003**, *154*, 533-558.
(23) Cao, T.; Song, Z.; Wang, S.; Xia, J. "A comparative study of the specific surface area and pore structure of different shales and their kerogens". *Sci. China: Earth Sci.* **2015**, *58*, 510-522.

(24) Abbe, E. "Beiträge zur Theorie des Mikroskops und der mikroskopischen Wahrnehmung". *Archiv für mikroskopische Anatomie* **1873**, *9*, 413-418.
(25) Chalmers, G. R.; Bustin, R. M.; Power, I. M. "Characterization of gas shale pore systems by porosimetry, pycnometry, surface area, and field emission scanning electron microscopy/transmission electron microscopy image analyses: Examples from the Barnett, Woodford, Haynesville, Marcellus, and Doig units". *AAPG Bull.* **2012**, *96*, 1099-1119.
(26) Saif, T.; Lin, Q.; Bijeljic, B.; Blunt, M. J. "Microstructural imaging and characterization of oil shale before and after pyrolysis". *Fuel* **2017**, *197*, 562-574.
(27) Kimble, B.; Maxwell, J.; Philp, R.; Eglinton, G.; Albrecht, P.; Ensminger, A.; Arpino, P.; Ourisson, G. "Tri-and tetraterpenoid hydrocarbons in the Messel oil shale". *Geochim. Cosmochim. Acta* **1974**, *38*, 1165-1181.
(28) Horsfield, B. "Practical criteria for classifying kerogens: some observations from pyrolysis-gas chromatography". *Geochim. Cosmochim. Acta* **1989**, *53*, 891-901.
(29) Van de Meent, D.; Brown, S. C.; Philp, R. P.; Simoneit, B. R. "Pyrolysis-high resolution gas chromatography and pyrolysis gas chromatography-mass spectrometry of kerogens and kerogen precursors". *Geochim. Cosmochim. Acta* **1980**, *44*, 999-1013.
(30) Anovitz, L. M.; Cole, D. R. "Characterization and analysis of porosity and pore structures". *Rev. Mineral. Geochem.* **2015**, *80*, 61-164.
(31) Kelemen, S.; Afeworki, M.; Gorbaty, M.; Sansone, M.; Kwiatek, P.; Walters, C.; Freund, H.; Siskin, M.; Bence, A.; Curry, D. "Direct characterization of kerogen by X-ray and solid-state 13C nuclear magnetic resonance methods". *Energy Fuels* **2007**, *21*, 1548-1561.
(32) Yang, J.; Hatcherian, J.; Hackley, P. C.; Pomerantz, A. E. "Nanoscale geochemical and geomechanical characterization of organic matter in shale". *Nat. Commun.* **2017**, *8*, 2179.
(33) Pettinger, B.; Ren, B.; Picardi, G.; Schuster, R.; Ertl, G. "Nanoscale probing of adsorbed species by tip-enhanced Raman spectroscopy". *Phys. Rev. Lett.* **2004**, *92*, 096101.
(34) Hao, Z.; Bechtel, H. A.; Kneafsey, T.; Gilbert, B.; Nico, P. S. "Cross-Scale Molecular Analysis of Chemical Heterogeneity in Shale Rocks". *Sci. Rep.* **2018**, *8*, 2552.
(35) Goodarzi, M.; Rouainia, M.; Aplin, A.; Cubillas, P.; de Block, M. "Predicting the elastic response of organic-rich shale using nanoscale measurements and homogenisation methods". *Geophys. Prospect.* **2017**, *65*, 1597-1614.
(36) Wang, L.; Wang, H.; Wagner, M.; Yan, Y.; Jakob, D. S.; Xu, X. G. "Nanoscale simultaneous chemical and mechanical imaging via peak force infrared microscopy". *Sci. Adv.* **2017**, *3*, e1700255.
(37) Kaemmer, S. B. "Introduction to Bruker's ScanAsyst and PeakForce Tapping AFM Technology (Bruker Application Note AN133, Bruker Nano Surfaces Division)". **2011**.
(38) Derjaguin, B.; Muller, V.; Toporov, Y. "On different approaches to the contact mechanics". *J. Colloid Interface Sci.* **1980**, *73*, 293-294.
(39) Pittenger, B. E., Natalia; Su, Chanmin. "Application Note #128 Quantitative Mechanical Property Mapping at the Nanoscale with PeakForce QNM". **2012**.
(40) Shawabkeh, R. A. "Adsorption of chromium ions from aqueous solution by using activated carbo-aluminosilicate material from oil shale". *J. Colloid Interface Sci.* **2006**, *299*, 530-536.
(41) Chen, Y.; Mastalerz, M.; Schimmelmann, A. "Characterization of chemical functional groups in macerals across different coal ranks via micro-FTIR spectroscopy". *Int. J. Coal Geol.* **2012**, *104*, 22-33.
(42) Painter, P. C.; Snyder, R. W.; Starsinic, M.; Coleman, M. M.; Kuehn, D. W.; Davis, A. "Concerning the application of FT-IR to the study of coal: a critical assessment of band

assignments and the application of spectral analysis programs". *Appl. Spectrosc.* **1981**, *35*, 475-485.
(43) Kim, S.; Kramer, R. W.; Hatcher, P. G. "Graphical method for analysis of ultrahigh-resolution broadband mass spectra of natural organic matter, the van Krevelen diagram". *Anal. Chem.* **2003**, *75*, 5336-5344.
(44) Okiongbo, K. S.; Aplin, A. C.; Larter, S. R. "Changes in Type II Kerogen Density as a Function of Maturity: Evidence from the Kimmeridge Clay Formation". *Energy Fuels* **2005**, *19*, 2495-2499.
(45) Zeng, Y.; Wu, C. "Raman and infrared spectroscopic study of kerogen treated at elevated temperatures and pressures". *Fuel* **2007**, *86*, 1192-1200.
(46) Liu, B.; Mastalerz, M.; Schieber, J. In *ACE 2018 Annual Convention & Exhibition*, 2018.
(47) Drollette, B. D.; Hoelzer, K.; Warner, N. R.; Darrah, T. H.; Karatum, O.; O'Connor, M. P.; Nelson, R. K.; Fernandez, L. A.; Reddy, C. M.; Vengosh, A. "Elevated levels of diesel range organic compounds in groundwater near Marcellus gas operations are derived from surface activities". *Proc. Natl. Acad. Sci.* **2015**, *112*, 13184-13189.
(48) Bolden, A. L.; Schultz, K.; Pelch, K. E.; Kwiatkowski, C. F. "Exploring the endocrine activity of air pollutants associated with unconventional oil and gas extraction". *Environ. Health* **2018**, *17*, 26.
(49) Llewellyn, G. T.; Dorman, F.; Westland, J. L.; Yoxtheimer, D.; Grieve, P.; Sowers, T.; Humston-Fulmer, E.; Brantley, S. L. "Evaluating a groundwater supply contamination incident attributed to Marcellus Shale gas development". *Proc. Natl. Acad. Sci.* **2015**, *112*, 6325-6330.
(50) Craddock, P. R.; Le Doan, T. V.; Bake, K.; Polyakov, M.; Charsky, A. M.; Pomerantz, A. E. "Evolution of kerogen and bitumen during thermal maturation via semi-open pyrolysis investigated by infrared spectroscopy". *Energy Fuels* **2015**, *29*, 2197-2210.
(51) Ganz, H.; Kalkreuth, W. "Application of infrared spectroscopy to the classification of kerogentypes and the evaluation of source rock and oil shale potentials". *Fuel* **1987**, *66*, 708-711.
(52) Kuo, L.-C. "Lower Cretaceous lacustrine source rocks in northern Gabon: effect of organic facies and thermal maturity on crude oil quality". *Org. Geochem.* **1994**, *22*, 257-273.
(53) Lis, G. P.; Mastalerz, M.; Schimmelmann, A.; Lewan, M. D.; Stankiewicz, B. A. "FTIR absorption indices for thermal maturity in comparison with vitrinite reflectance R0 in type-II kerogens from Devonian black shales". *Org. Geochem.* **2005**, *36*, 1533-1552.
(54) Ferralis, N.; Matys, E. D.; Knoll, A. H.; Hallmann, C.; Summons, R. E. "Rapid, direct and non-destructive assessment of fossil organic matter via microRaman spectroscopy". *Carbon* **2016**, *108*, 440-449.
(55) Li, C.; Ostadhassan, M.; Guo, S.; Gentzis, T.; Kong, L. "Application of PeakForce tapping mode of atomic force microscope to characterize nanomechanical properties of organic matter of the Bakken Shale". *Fuel* **2018**, *233*, 894-910.
(56) Washburn, K. E.; Birdwell, J. E. "Multivariate analysis of ATR-FTIR spectra for assessment of oil shale organic geochemical properties". *Org. Geochem.* **2013**, *63*, 1-7.
(57) Dodsworth, P. "Palynostratigraphy and palaeoenvironments of the Eagle Ford Group (Upper Cretaceous) at the Lozier Canyon outcrop reference section, west Texas, USA". *Palynology* **2016**, *40*, 357-378.
(58) Van Krevelen, D. W. "Organic geochemistry—old and new". *Org. Geochem.* **1984**, *6*, 1-10.
(59) Killops, S. D.; Funnell, R. H.; Suggate, R. P.; Sykes, R.; Peters, K. E.; Walters, C.; Woolhouse, A. D.; Weston, R. J.; Boudou, J. P. "Predicting generation and expulsion of paraffinic oil from vitrinite-rich coals". *Org. Geochem.* **1998**, *29*, 1-21.

(60) Dazzi, A.; Prater, C. B.; Hu, Q.; Chase, D. B.; Rabolt, J. F.; Marcott, C. "AFM-IR: combining atomic force microscopy and infrared spectroscopy for nanoscale chemical characterization". *Appl. Spectrosc.* **2012**, *66*, 1365-1384.

For Table of Contents Only